CMT Ceramics in Modern Technologies
Techna Group srl

Copyright © Techna Group S.r.l., Faenza, Italy

Improvement of Optical and Mechanical Properties, and Controlled Release of Drug Delivery Powder Cosmetics

Yasumasa Takao[a]*, Naoaki Toyoda[b], Tsuyoshi Asai[c], Toshihiko Okadera[b], Hiroyuki Asano[b]
[a]National Institute of Advanced Industrial Science and Technology (AIST), Shimoshidami, Nagoya, Aichi, Japan; [b]Research Laboratories, Nippon Meanard Cosmetic Co., Ltd., Nagoya, Japan; [c]Sanshin Mining Ind. Co., Ltd., Aichi, Japan

Through collaboration between industry and government, we succeeded in blending synthetic seeds, evaluation seeds, and cosmetics needs and quickly established original products and sensibility studies. By controlling the average inter-surface distance in the liquid and the surface/volume precipitation in the droplet, it was possible to prepare composite particles, hollow granules and drug-encapsulating granules. Control of these microstructure improved UV shielding and optical sharpness and allowed obtaining several sustained release rates of the drug. Systematic verification of the direct shear testing method and organoleptic evaluation promoted the association between qualitative sensory parameters and physical properties and, furthermore, the standardization of the test method. Through collaboration among academia, industry and government in the powder technology field, authentication assessment (i.e., ISO, JIS) of the test methods was established.

Keywords: Cosmetics, Beads milling, Spray drying, Shear testing, UV shield, Smoothness.

1. Introduction

In a global environment of change and aging progression, one of the photoaging measures is makeup cosmetics. However, raw mica and nano-TiO_2 nanoparticles are easy to cohere, and the transparency and lubricity characteristics are lapsed only by merely mixing them. The quantification of a sensitivity study to give good usability and photoaging measures for ultraviolet (UV) rays are needed.

Figure 1 shows an apparent limit of making a cosmeceutical pearl-pigment powder. It is a composite-particle consisting of $KAl_2AlSi_3O_{10}(OH)_2$ mica raw material and TiO_2 [1-4]. Generally, TiO_2, the UV shielding agent, is a superfine particle (nanoparticle) having diameters of 0.01-0.1 μm. Mica, a scale-like (plated structure) clay mineral particle, is 1-100 μm long and 0.1-1 μm thick (see the aspect-ratio in Fig. 2). Superfine and plated particles face difficulties in reducing their own aggregation before making a composite microstructure by surface attraction (i.e., van der Waals force). Therefore, to disperse uniformly with each other, a dispersing chemical (e.g., surfactant) is indispensable. Even when using chemicals, a composite particle could not be made completely [5-10].

Figure 2 shows the existing products map of pear pigment. Apparently, there is a technological limit for the prior arts, e.g., IRIODIN® (MERCK Co., Inc.), COVERLEAF® (JGC CATALYSTS AND CHEMICALS Ltd.), SILSEEM® (NIHON KOKEN KOGYO Co., Ltd.), and NABEYAMA Mica (HIKAWA KOGYO Inc.) [1-4]. These pearl pigment materials' performances depend on the particle-size (both mica & TiO_2) and aspect ratio of mica. The smaller the TiO_2 size is, the higher the UV-B shielding; however, there is considerable aggregation in the superfines. The smaller the aspect ratio of mica is, the higher the powder molding strength and smooth impression from the use of a powder foundation cosmetic product; however, it is difficult to make the smaller ratio [1-4].

We propose (1) FURIKUSA mica having an unprecedented smaller aspect-ratio, (2) UV shielding products having a particle size of 50 nm and aspect ratio of 10 (Nanocomposite), and (3) 5-μm granulated powder consisting of 50-nm nanoparticles (Nanosphere) [11-13].

2. Experimental

Figure 3 shows our scheme of spraying, beads milling and numerical calculation. Figure 4 indicates the detail of the numerical calculation to decide the threshold of TiO_2 addition amounts. To disperse nanoparticles uniformly and prevent their aggregation, the threshold is under 10 vol% for 20-nm TiO_2, and over 30vol% is possible in the 50-nm case [11-13].

2.1. Slurry preparation (numerical calculation and beads-milling)

As shown in Fig. 3, nanoparticles are attracted and/or repulsed by van der Waals' attraction force and electrostatic repulsion (and/or attraction) forces, simultaneously. When an excessive amount of nanoparticles is loaded, the nanoparticles begin to contact each other, i.e., aggregate.

Figure 4 shows the potential barrier calculated from the attractive potential by van der Waals' force and the electrostatic repulsive potential. Interparticle distances (L_{DLVO} and $L_{Woodcock}$ in Fig. 4) are calculated by assuming a hexagonal close-packed structure compared with the nanoparticle loading amounts [11-13].

The DLVO (Professors B. Derjaguin, L. Landau, E. Verwey and T.

* *Corresponding author*
E-mail address: lilliput@ni.aist.go.jp

https://doi.org/10.29272/cmt.2018.0005
Received July 10, 2018; Received in revised form September 12, 2018; Accepted September 12, 2018

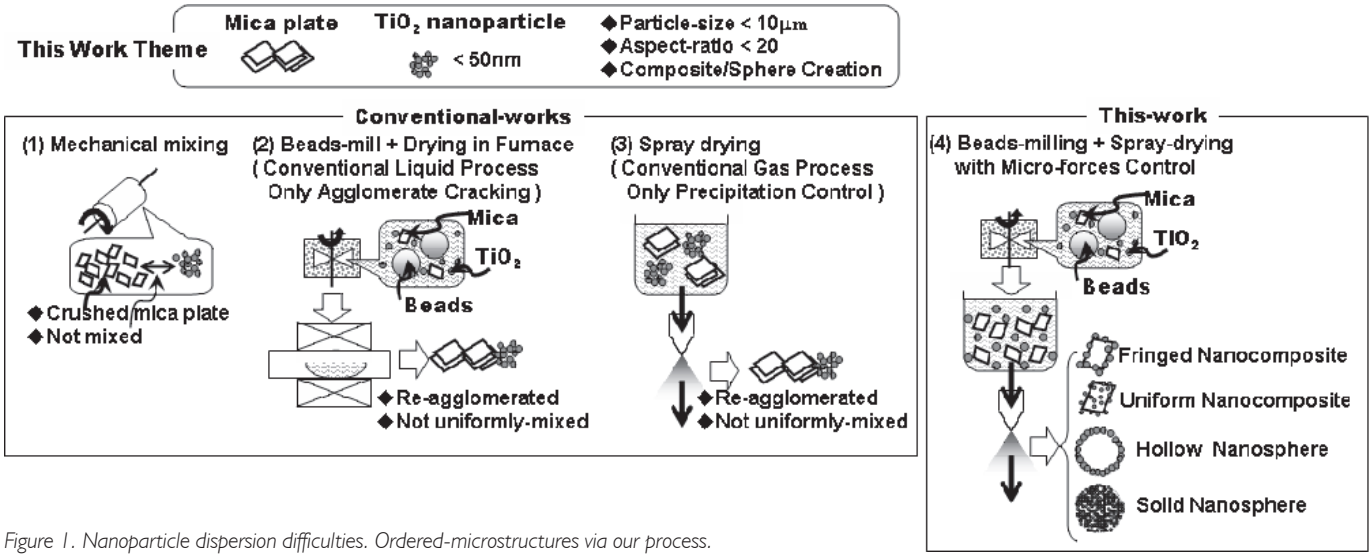

Figure 1. Nanoparticle dispersion difficulties. Ordered-microstructures via our process.

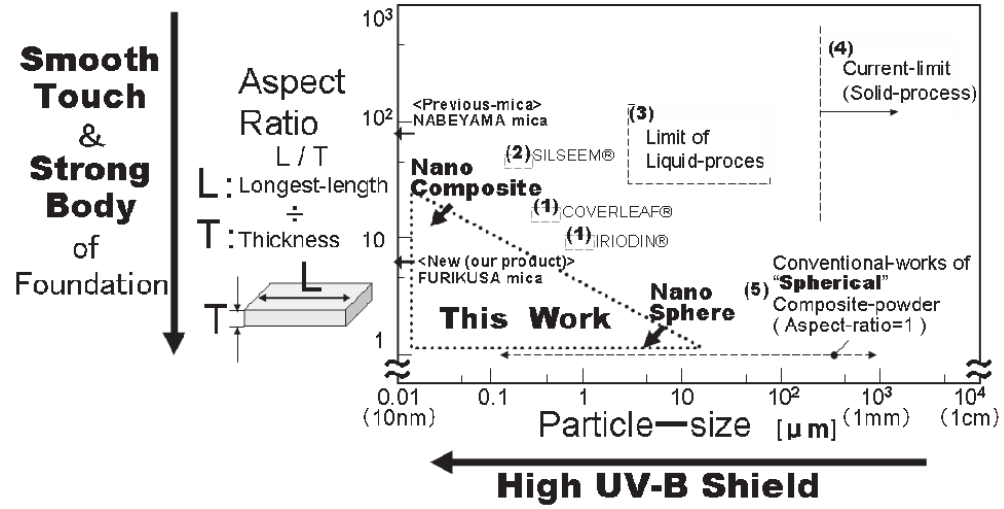

Figure 2. Existing pearl-pigment products and their aspect-ratio & particle-size maps.

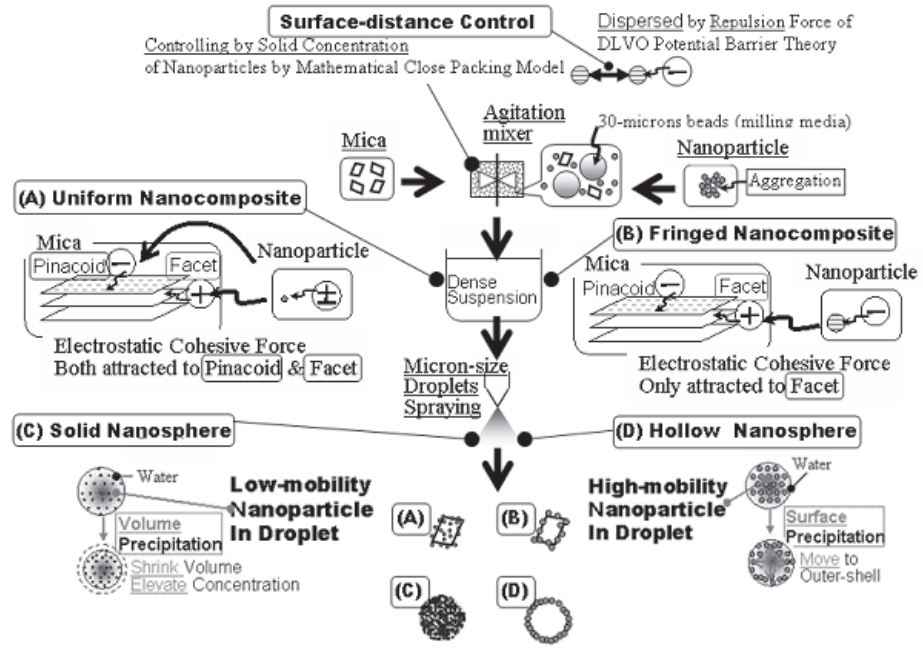

Figure 3. Scheme of spraying, beads-milling and numerical calculation.

Overbeek) theory [14] allows for dispersing particles based on the electrostatic potential barrier. The theory shows that above a potential barrier value of 15, the loaded particles disperse without aggregation (Fig. 4). However, in the case of nanoparticles, their uniform dispersion is difficult using only the DLVO interactions because of their relatively small potential barrier (the effect of van der Waals' attraction force is relatively large). L_{DLVO}, a limit of allowable loading amount for uniform dispersion, is very short, i.e., a few nanometers, so it only works for a very low concentration of nanoparticles.

Woodcock first reported the relationship between the nanoparticle volume fraction (concentration of solid loading amounts) and their interparticle distances, i.e., the non-equilibrium molecular dynamics (NEMD) method [10-13, 15].

In Fig. 4, the model shows that the nanoparticles form an aggregate when overloading larger than the volume fraction, which is calculated from the interparticle distance, i.e., $L_{Woodcock}$. The NEMD method describes that the L_{DLVO} of 20-nm TiO2 is a few nanometers under the 10 vol% solid loading. Apparently, to disperse nanoparticles without aggregation, the threshold is under 10 vol% for 20 nm TiO_2. On the other hand, the L_{DLVO} of 50 nm TiO_2 is over 10 nm. In this case, we can fill over 30 vol% [11-13].

Further, we first applied an accelerated flow field theory to this nanoparticle dispersion model [11-13]. Generally, a dispersion of agglomerated particles in the accelerated flow field (i.e., beads-

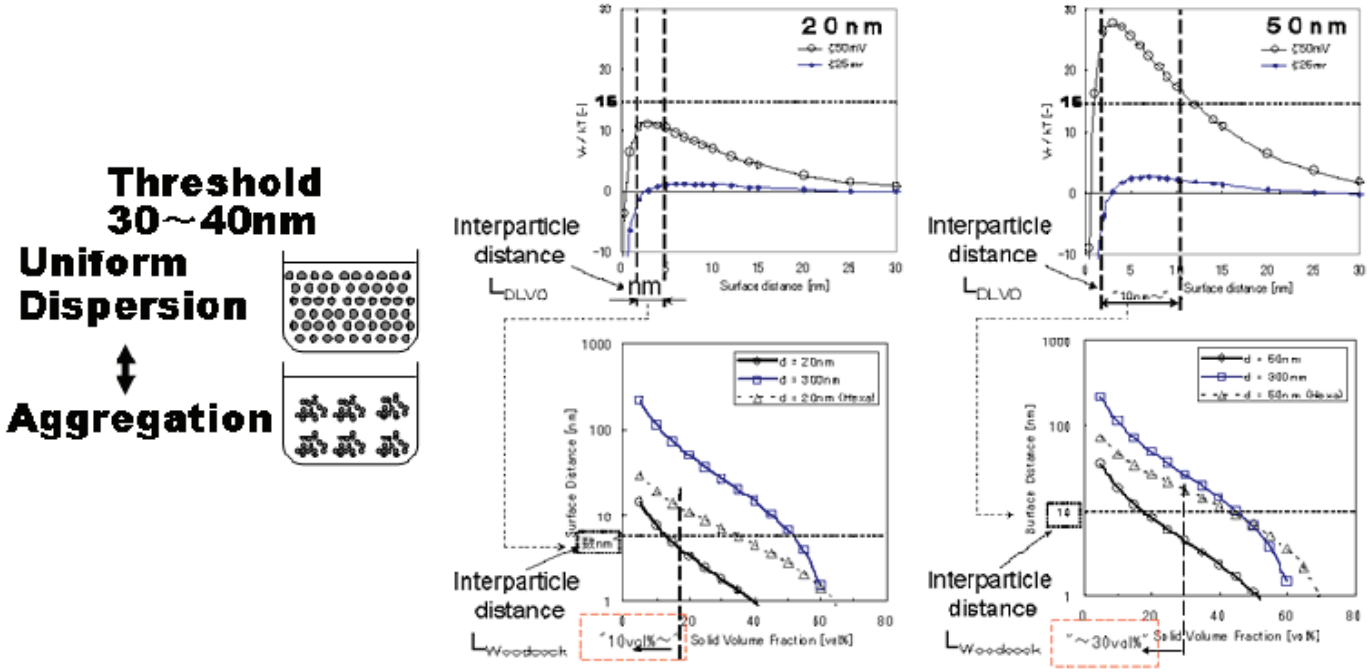

Figure 4. Numerical calculation to disperse TiO2 nanoparticles and prevent their aggregation.

milling) utilizes two micro dispersion forces: (1) resistance of the particle to the flow and (2) inertial force [16, 17]. Surface force (capillary, electrostatic) is proportional to the diameter, resistance to flow (cross-sectional area) is proportional to the square of the diameter, and inertia (gravity) is proportional to the cube of the diameter. At less than around 5 μm, the influence of the surface is dominant compared to the inertia. We applied 20 nm TiO_2 with no electrostatic charge and 50 nm TiO_2 with negative electrostatic charge (Fig. 3). In conclusion, the electrostatic and resistance forces of the 50 nm particles are larger than those of the 20 nm particles, i.e., the 50 nm particles have a higher "MOBILITY."

We applied the NEMD method and the accelerated flow field theory to make a composite particle and a granule composed of nanoparticles [11-13]. The nanocomposite shown in Fig. 3(A) in which TiO_2 nanoparticles are coated on the mica plate uniformly is made by 20 nm TiO_2 with no electrostatic charge. The solid-core sphere (Fig. 3(C)) is also prepared by 20 nm TiO_2 to lower the nanoparticle mobility in the slurry.

Meanwhile, the composite of nanoparticles coated on only around the fringe of mica in Fig. 3(B) and the hollow nanosphere in Fig. 3(D) are made by 50 nm TiO_2 with negative electrostatic charge. Using high mobility nanoparticles to move rapidly onto the mica facet that is positively charged, we can create these anisotropic composite microstructures (Figs. 3(B)(D)) as described below [11-13].

Beads milling (UAM015, KOTOBUKI KOGYO Ltd.) disperses nanoparticles uniformly and prevents their aggregation using ZrO_2 plasma beads (D50 = 30 μm, DAIKEN CHEMICAL Co., Ltd.). The TiO_2 (50 nm, MT500H, TAYCA Co.; 20 nm, TTO-51, ISHIHARA SANGYO KAISHA Ltd.) loading in distilled water is 2 vol%. In this case, $L_{Woodcock} < L_{DLVO}$ is satisfied nicely even in Fig. 4 severe case (i.e., 20 nm). It can distribute nanoparticles uniformly and prevent their aggregation [11-13]. Subsequently, FURIKUSA mica (7 μm, Sericite, FSE, SANSHIN MICA Co.) is mixed with the nanoparticle slurry (50 vol% solid loading).

2.2. Spraying

Spray drying (MDL-050B, FUJISAKI ELECTRIC Co. Ltd.) creates a well dispersed single micron droplet by a triple fluid nozzle (PN3005, FUJISAKI ELECTRIC Co. Ltd.). The droplet includes only one 7 μm mica coated with nanoparticles (Fig. 3(A),(B)). This micron-sized droplet is essential for controlling the nanoparticle coating condition. Also, it can lead to a narrow size distribution of granules consisting of the nanoparticles (Fig. 3(C),(D)) [11-13].

Volume precipitation [5] is dominant in the case of lower mobility of nanoparticles in the slurry (Figs. 3(A),(C)). This low mobility enables the gradual shrinkage of droplets. This gradual shrinkage allows the neutral charged 20nm TiO_2 nanoparticles to coat all over the mica plate uniformly (Fig. 3(A)). Also, the gradual shrinkage makes a higher densified solid nanosphere during its sufficiently long drying period (Fig. 3(C)).

Surface precipitation [5], meanwhile, is a central part of the higher mobility (Figs. 3(B),(D)). A higher value shrinks the droplets rapidly. This rapid shrinkage drives the solute to move to the droplet surface. Thus, this higher mobility aggravates the 50 nm TiO_2 with a negative electrostatic charge to attach onto the positively-charged mica facet (Fig. 3(B)). Also, the rapid shrinkage causes a cavity in the lower-densified hollow granule during the considerably shorter drying time (Fig. 3(D)).

2.3. Evaluations

Mesostructures of the composite particle and granule are confirmed by analytical electron microscopy (AEM) and scanning electron microscopy (SEM).

A spectrophotometer (UV160A, SHIMAZU Co.) is used to indicate the transmissivity (among 290~800 nm) of a silicon film representing the human skin that our prepared powders are put on.

The shear properties of compacted powder (NS-S200, NANO SEEDS Co.) represent a variety of feeling textures of cosmetic powder foundation. The granule crushing strength (NS-A100, NANO SEEDS Co.) is also measured to collect supporting evidence of the feeling texture [11-13].

3. Results & discussion

3.1. Mesostructures (a diversity to design cosmeceutical performances)

Figure 5 shows the nanocomposites and nanospheres shown in Fig. 3(A)-(D). "Uniform nanocomposite" in Fig. 5(A) indicates

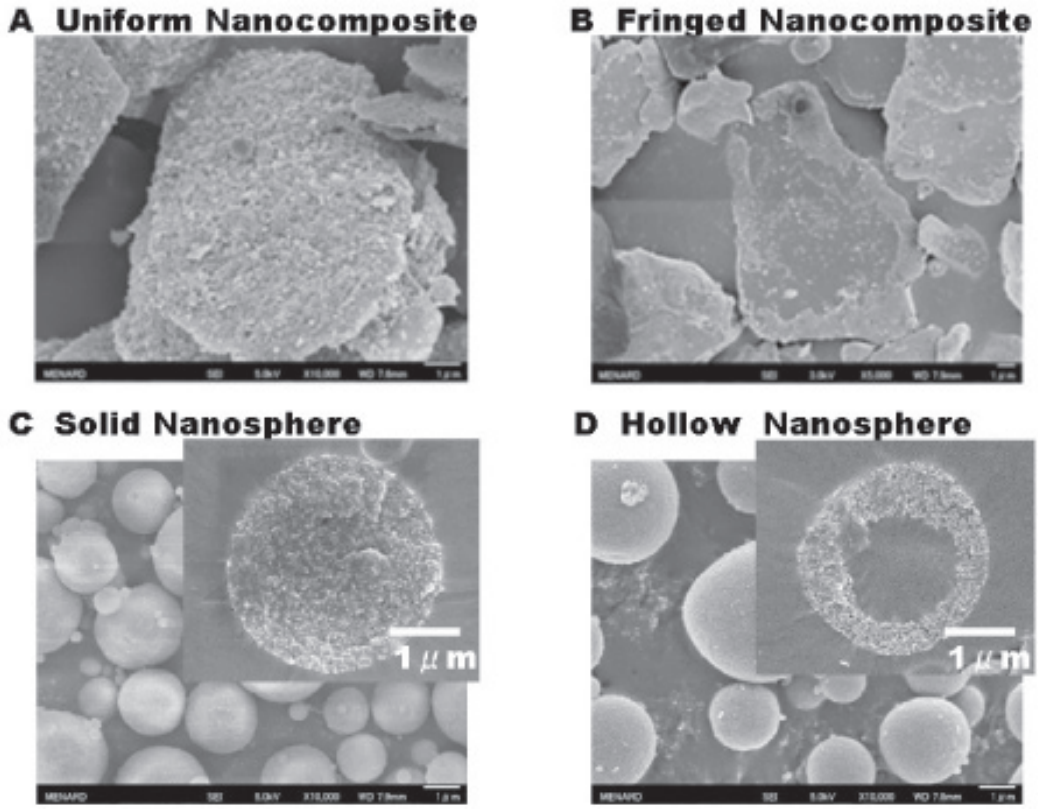

Figure 5. Nanocomposites: (A) uniform, (B) fringed, and nanospheres: (C) solid, (D) hollow.

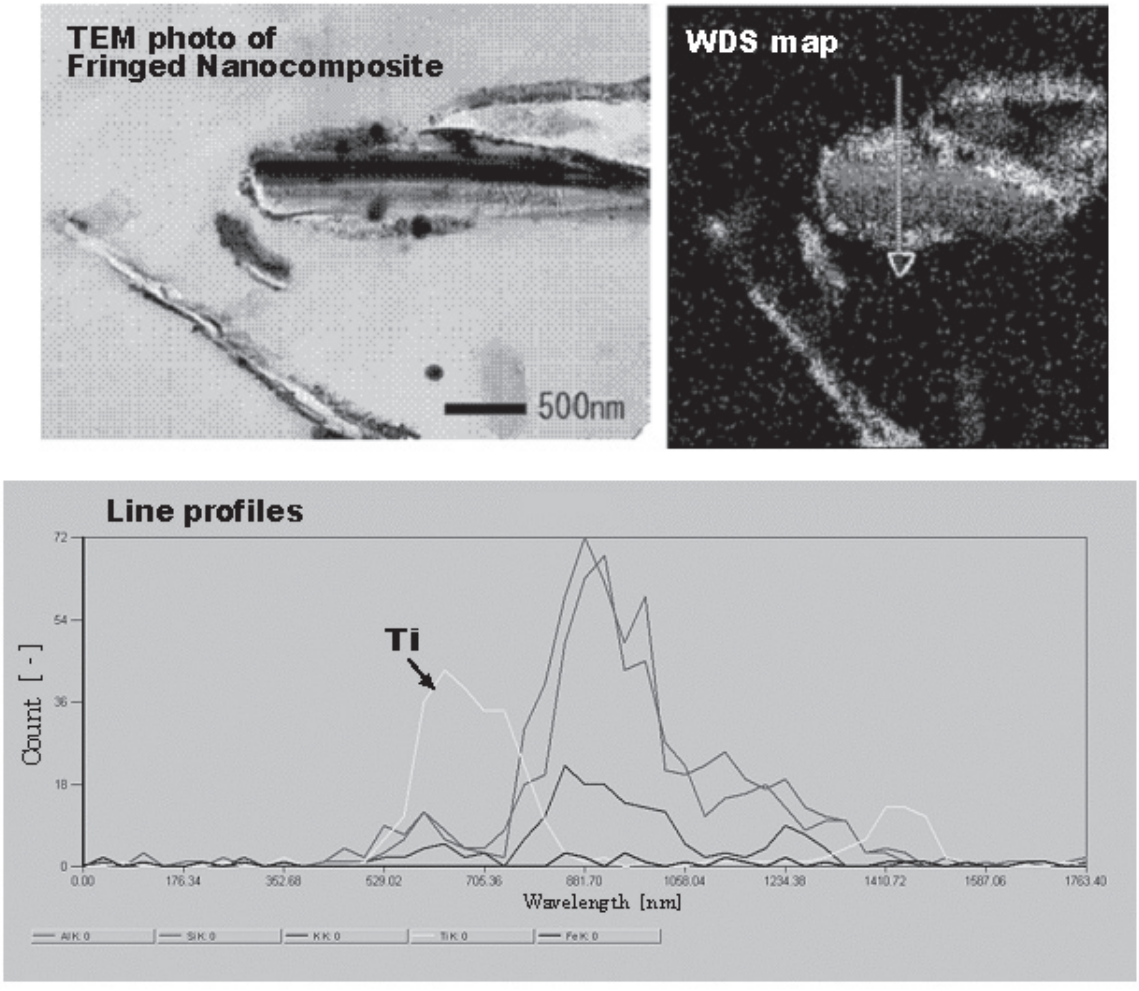

Figure 6. AEM photos and line profile of fringed nanocomposite (Fig. 5(B)).

50 nm TiO_2 nanoparticles coated on 7 μm mica-plate uniformly. "Fringed nanocomposite (Fig. 5(B))" demonstrates the composite microstructure of nanoparticles coated only around the facet of the mica.

The AEM photos and line profile in Fig. 6 demonstrate no mica pinacoid. The Ti component is only detected at both ends of the other components (Si, Al, K and Fe). The line profiles reveal that the composite of nanoparticles coated only around the fringe of the mica, shown in Fig. 3(B), is created.

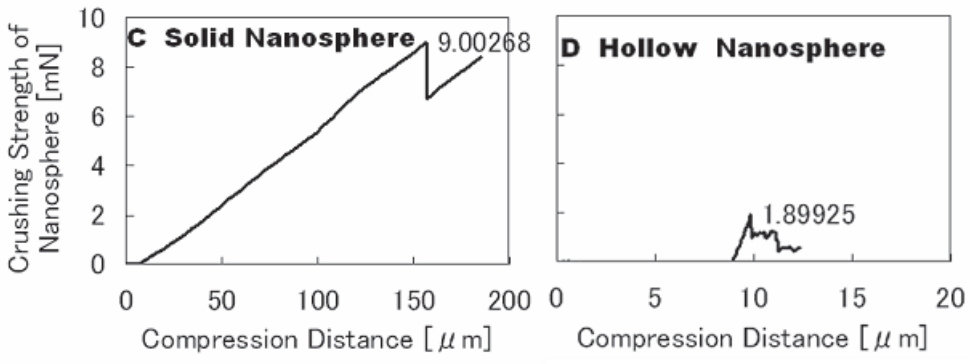

Figure 7. Granule crushing strength of solid (Fig. 5(C)) and hollow (Fig. 5(D) spheres.

"Solid-core sphere" of 20 nm TiO_2 nanoparticles is shown in Fig. 5(C). "Hollow nanosphere (Fig. 5(D))" having a 1 μm cavity in the granule microstructure is prepared by 50 nm TiO_2.

Figure 7 shows the granule crushing strengths. The solid nanosphere (Fig. 5(C)) reaches the higher strength and compression distance by the crushing force. These higher values depend on the smaller (20 nm) nanoparticles and higher granule density (i.e., no hollow). We can select the nanospheres (Fig. 3(C),(D)) according to the need of the feeling texture of cosmetic powder foundation.

The mesostructures shown in Figs. 5-7 illustrate the diversity of nanocomposite and nanosphere constructions attainable by our method.

3.2. UV protection and transparency

Figure 8 shows the shielding ability in the UV light region and transparency in the visible light region. Figure 8(a) shows our human skin model prepared by the nanocomposite (Figs. 5(A),(B)). Figure 8(b) is a powder foundation consisting of a commercialized powder for UV protection (COVERLEAF®, JGC CATALYSTS AND CHEMICALS Ltd.). Figure 8(c) is the result of a silicon film dispersed with mica raw powder (for reference).

The desired ideal state is the lower light transparency in the UV range, especially in the UV-B field of 280-315 nm for sun protection factor. Simultaneously, high transparency is indispensable under the visible light region of 380-780 nm. Then, a sharp drop in transparency from the visible to the UV range is a performance index of the UV shielding ability. Figure 8(a), i.e., our model prepared by blending the nanocomposite (Figs. 5(A),(B)), shows the sharp-drop performance. It depends on a combination of 2 effects. (1) First, the "Uniform nanocomposite (Fig. 5(A))" shields enough UV light (but also visible light). (2) Second, the "Fringed nanocomposite (Fig. 5(B))" puts visible light through (but less UV protection). The combination creates the sharp-drop performance from the visible to the UV range.

Meanwhile, the previous powder foundation is insufficient for UV protection and visible transparency (Fig. 8(b)) because of a large amount of TiO_2 nanoparticle aggregation. This aggregation is unavoidable via the conventional preparation method as analyzed in Fig. 2. The nanoparticle agglomerate deteriorates the efficiency of UV protection and opacifies visible transparency.

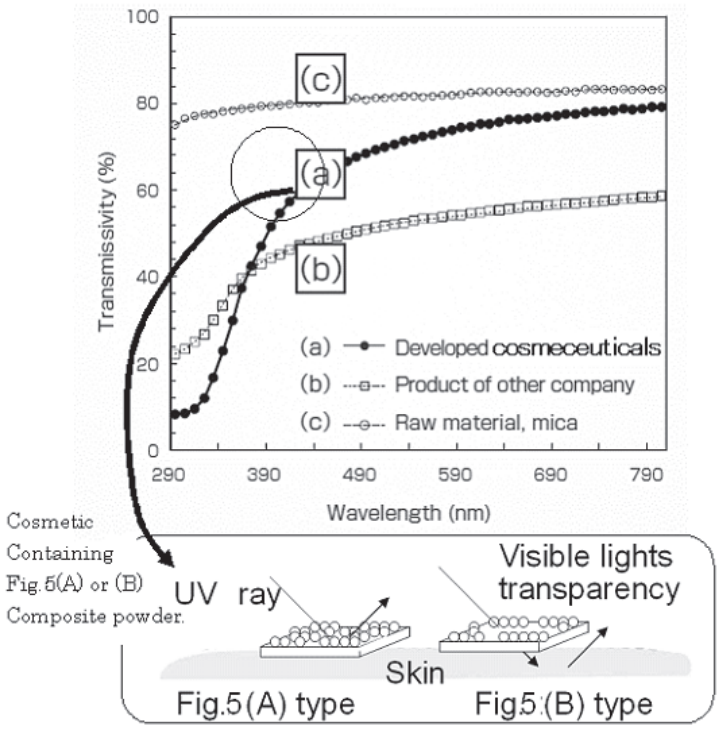

Figure 8. Shielding ability in the UV light region and transparency in the visible light region.

3.3. Feeling textures of cosmetic powder-foundation

Figure 9 shows a variety of feeling textures of cosmetic powder foundation and the collapsing behavior of powder bed: (a) silicone-treated sericite, (b) silicone-treated sericite-TiO_2, (c) stearic-acid treated sericite-TiO_2, (d) powdery mixture

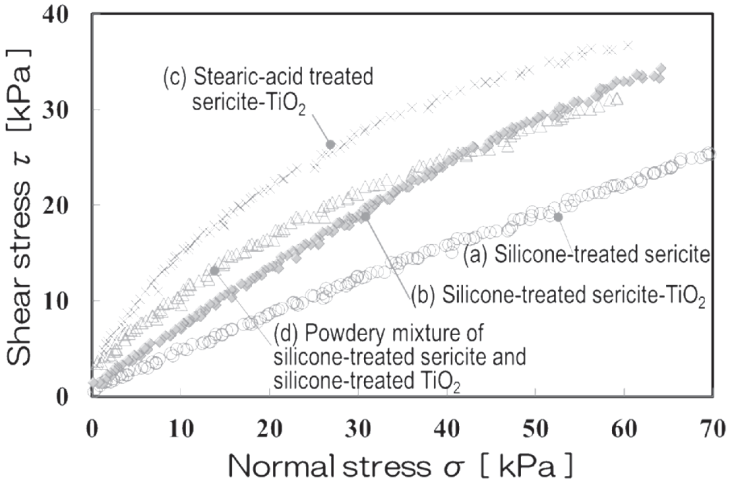

Figure 9. Feeling textures of cosmetic powder-foundation.

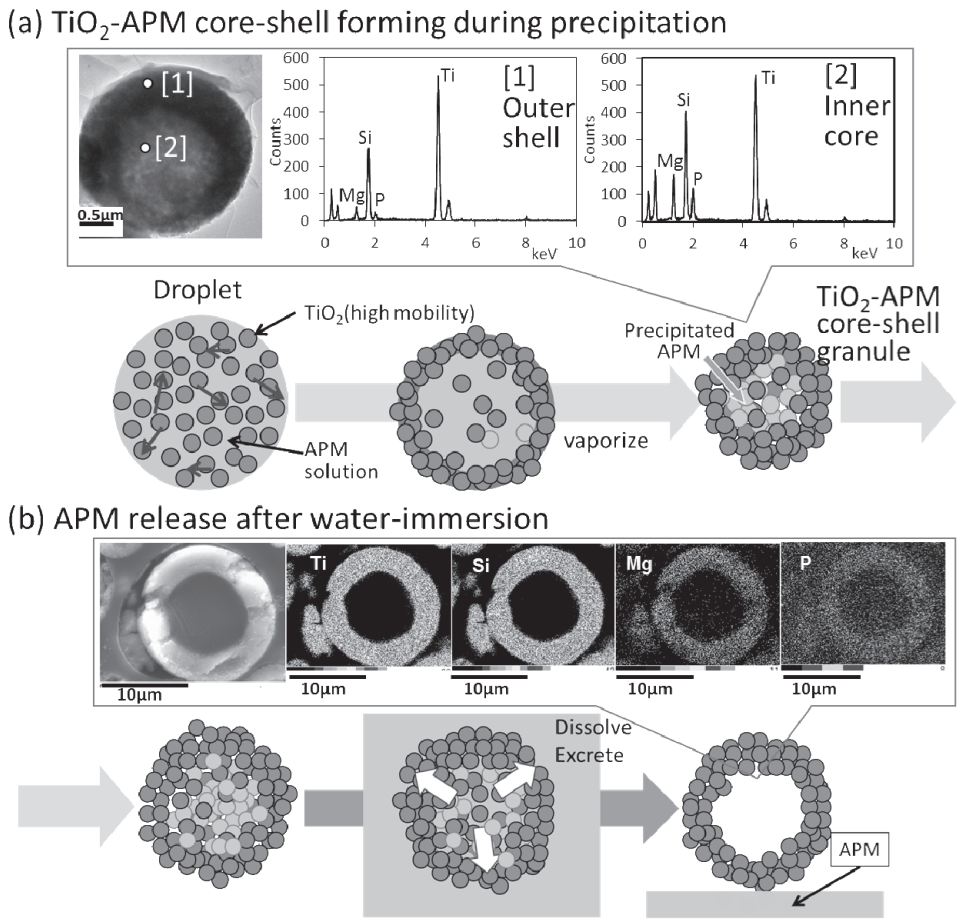

Figure 10. Controlled-release drug including the granular chemical.

of silicone-treated sericite and silicone-treated sericite-TiO_2.
A silicone treatment is generally used when we wish to enhance the slipping feeling textures of cosmetic powder foundation. Figure 9(a), (b) show that the silicone-treated powders represent a straight line passing through an origin. This means that the powders are a nonadherence Coulomb powder.
A stearic acid treatment is used when the desire is to enhance the moist feeling texture of cosmetic powder foundation. Figure 9(c) shows that the stearic-acid-treated powder has a y-intercept and curvature in the graph. This means that the powder is an adherence non-Coulomb powder.
Figure 9(d) is a mixed powder of silicone-treated powders. The slipping feeling texture of the mixed powder is lower than that of the composite powder (Figure 9(b)). This suggests that the nanoparticles that detached from the surface of the composite powder have keenly affected the texture feeling of the cosmetic powder foundation.
We first reveal that a shear testing method used in the field of ceramic compact is useful to reveal a variety of qualitative feeling textures of cosmetic powder foundation.

3.4. Controlled-release drug delivery

Figure 10 shows the morphology changes of the controlled-release drug including the granular chemicals: (a) TiO_2-APM core-shell forming during precipitation (TEM-EDX analysis: cross-sectional image, element-distribution spectra of Ti, Si, Mg and P, at [1] outer-shell and [2] inner core), (b) APM release after water immersion (SEM-EDX analysis: cross-sectional image, element distribution mapping of Ti, Si, Mg and P).
The outer shell has the Ti element, and the inner-core includes the Mg element. This means that TiO_2-APM core-shell formation is enabled as shown in Figure 10(a).

Figure 10(b) shows an example of the controlled-release drug delivery for powder cosmetics. After water immersion of the TiO_2-APM core-shell (Figure 10(a)), the Mg element in the inner core is dismissed. This means that APM release has been realized.

4. Conclusion

By controlling the average inter-surface distance in the liquid and the surface/volume precipitation in the droplet, it was possible to prepare a composite particle, hollow granule and drug-encapsulating granule. Control of these microstructure improved the UV shielding and the optical sharpness and allowed to obtain the controlled release of vitamin C (L-ascorbic acid 2-phosphate magnesium, $C_6H_7MgO_9P$, APM) on human skin. Systematic verification of the direct shear testing method and organoleptic evaluation between the qualitative sensory parameters and physical properties reveal that a shear testing method used in the field of ceramic compacts is useful for revealing a variety of feeling textures of cosmetic powder foundation.

References

[1] Du Pont., Micaceous Flake Pigment, USA patent 3087827 (1963).
[2] T. Miyazaki, "COVERLEAF®" Characteristics of Highly Functional Inorganic Particles in Cosmetic Field, Technol. Report JGC Catalysts and Chemicals Ltd., 17, 67-74 (2000).
[3] F. Suzuki, Y. Murui, M. Adachi, K. Hashimoto and Y. Toda, "SILSEEM®" Preparation of Interference Colors and High Luster Pearlescent Pigments Provided by Thin Film Laminations with Different Refractive Index, J. Jpn. Soc. Colour Mater., 81, 429-436 (2008).
[4] T. Hoshino, "IRIODIN®" Pigments using Principles of Optical Interference Colors, J. Jpn. Soc. Colour Mater., 84, 246-253 (2011).
[5] G. L. Messing, S. Zhang and G. Jayanthi, Ceramic Powder Synthesis by Spray Pyrolysis, J. Am. Ceram. Soc., 76, 2707-2726 (1993).
[6] W. Walker, J. Reed and S. Verma, Influence of Slurry Parameters on the Characteristics of Spray-dried Granules, J. Am. Ceram. Soc., 82, 1711-1719 (1999).
[7] G. Bertranda, C. Filiatreb, H. Mahdjouba, A. Foissyb and C. Coddeta, Influence of Slurry Characteristics on The Morphology of Spray-Dried Alumina Powders, J. Eur. Ceram. Soc., 23, 263-271 (2003).
[8] Y. Kamata and H. Oka, Development of Multifunctional Marimo Shaped Titanium Dioxide and Application as A Cosmetic Ingredient, FRAGRANCE J., 35 (No.3), 45-49 (2007).
[9] M. Tanaka, Preperation of Fine Composite Particles by Suspension Polymerization, J. Jpn. Soc. Colour Mater., 82, 23-29 (2009).

[10] M. Iijima, M. Tsukada and H. Kamiya, Effect of Particle Size on Surface Modification of Silica Nanoparticles by using Silane Coupling Agents and Their Dispersion Stability in Methylethylketone, Journal of Colloid and Interface Science, 307, 418-424 (2007).
[11] Y. Takao and M. Sando, Products and Evaluation Device of Cosmetics for UV Protection (AIST Commercialization based on regional Collaboration that Combines The Current Strategic Logic, and An Intermediary'S Experience and Trial-and-Error Approach), Synthesiology English Edition 3(No.2), 140-150 (2010).
[12] Y. Takao, T. Asai, H. Asano, K. Tsubata, T. Okuura and S. Nakata, Production-method and Apparatus of Composite-particle and Granules by Adhering Nanoparticles and Loosening their Aggregation, Japan-patent 2011-116569 (2011).
[13] Y. Takao, T. Asai, T. Okuura, N. Toyoda, M. Oda and H. Asano, J. Soc. Cosmet. Chem. Jpn., 50 (No.2), 113-119 (2016).
[14] E.J.W. Verwey, Theory of the Stability of Lyophobic Colloids, J. Phys. Chem., 51 (No.3), 631-636 (1947).
[15] L.V. Woodcock, Entropy Difference between the Face-centred Cubic and Hexagonal Close-packed Crystal Structures, Nature, 385, 141-142 (1997); Molecular dynamics and relaxation phenomena in glasses, Proc. a workshop held at the Zentrum für Interdisziplinäre, Forschung Universität Bielefeld, 277, 113-124 (1987).
[16] Y. Kousaka, Y. Endo, T. Horiuchi and T. Niida, Dispersion of Aggregate Particles by Acceleration in Air Stream, J. Chem. Eng. Jpn., 18, 233-239 (1992).
[17] Y. Endo and Y. Kousaka, Dispersion mechanism of coagulated particles in liquid flow, Colloids and Surfaces A: Physicochemical and Engineering Aspects, 109, 109-115 (1996).